Polymer Chemistry

PAPER

View Article Online
View Journal | View Issue

Check for updates

Cite this: *Polym. Chem.*, 2019, **10**, 1498

Encapsulating an organic phase change material within emulsion-templated poly(urethane urea)s†

Liora Weinstock,‡ Rajashekharayya A. Sanguramath *‡ and Michael S. Silverstein *

Received 5th December 2018,
Accepted 7th February 2019

DOI: 10.1039/c8py01733f

rsc.li/polymers

PolyHIPEs (PHs) are usually porous polymer monoliths templated within high internal phase emulsions (HIPEs), emulsions containing at least 74% dispersed internal phase, through free radical polymerization. Truly closed-cell PHs for encapsulating water, aqueous solutions, or inorganic salts have been synthesized within water-in-oil HIPEs through a judicious selection of HIPE formation and polymerization conditions. Encapsulating organic phase change materials such as octadecane (OD), within PHs would be advantageous for thermal energy storage and release applications. Here, exceptionally large amounts (~90 wt%) of OD were encapsulated as micrometer-scale capsules within poly(urethane urea) (PUU) PHs that were synthesized within oil-in-water HIPEs *via* interfacial step growth polymerization. The PUU was based on tannic acid (polyol) and sodium alginate (reactive surfactant), both in the aqueous external phase, and an isocyanate in the organic internal phase. The PH synthesized using hexamethylene diisocyanate (HDI), exhibited a relatively high thermal energy storage capacity (211 J g_{sample}^{-1}), a thermal behavior that was significantly different from that of OD, and robust mechanical behavior. It is the more flexible macromolecular structure produced with HDI that enables the successful encapsulation of the OD and the associated efficient thermal energy storage and robust mechanical behavior.

Published on 08 febrero 2019. Downloaded on 24/10/2025 02:32:36 a. m..

Introduction

A polyHIPE (PH) is a polymer monolith that is usually templated within a high internal phase emulsion (HIPE), an emulsion containing at least 74% dispersed internal phase, by polymerizing monomers in the external phase.[1–4] PHs are usually prepared *via* thermally initiated free radical polymerization, while other polymerization chemistries such as controlled radical polymerization,[5–8] step growth polymerization (SGP),[9,10] and ring-opening polymerization are rarely applied.[2] Emulsion templating enables access to a wide variety of molecular architectures and complex PH systems including semicrystalline PHs,[11] bicontinuous hydrophobic–hydrophilic PHs,[12] hybrid organic–inorganic PHs,[13–16] interpenetrating polymer network PHs,[17] inorganics,[18,19] nanocomposites,[20–23] and precursors for porous carbons.[24–28] PHs usually have highly interconnected open-cell morphologies, and under certain synthesis conditions, they can also have truly closed-cell morphologies.[8] Open-cell PHs with tunable porosities are useful for a wide range of applications such as tissue engineering scaffolds,[29–33] catalyst supports,[34–36] water purification,[37,38] shape memory foams,[39–41] and separations.[42,43] The synthesis of closed-cell PHs able to store useful organic liquids and melts within micrometer-scale capsules is just beginning to be explored.[44,45]

Truly closed-cell PHs for encapsulating water, aqueous solutions, or inorganic salts have been synthesized within water-in-oil (w/o) HIPEs through a judicious selection of the locus of initiation (interfacial *vs.* external-phase),[46] the stabilization strategy (surfactants *vs.* nanoparticles),[47–50] the internal phase volume fraction,[51] and the polymerization chemistry.[2] The structures of many PHs can appear to be closed-cell based upon scanning electron microscopy (SEM).[7,50] However, in most cases, the internal phase can easily be removed using vacuum drying or lyophilization, suggesting that interconnectivity does exist on the nanoscale. Elastomers that encapsulated up to 85% water in discrete micrometer-scale capsules were produced within w/o Pickering HIPEs using interfacially initiated free radical polymerization.[8] These PHs exhibited outstanding water retention, losing only 50% of the stored water through evaporation in 127 days, and exhibited excellent self-extinguishing fire retardation. The conditions for achieving truly closed-cell structures were relatively restrictive and included both using nanoparticle-based HIPE stabilization and using interfacially initiated free radical polymerization.

Department of Materials Science and Engineering, Technion – Israel Institute of Technology, Haifa 32000, Israel. E-mail: rsangurmath@gmail.com, michaels@technion.ac.il; Fax: +972-77-887-1797; Tel: +972-4-829-4582

†Electronic supplementary information (ESI) available. See DOI: 10.1039/c8py01733f

‡Contributed equally to this work.

This journal is © The Royal Society of Chemistry 2019

Published on 08 febrero 2019. Downloaded on 24/10/2025 02:32:36 a. m..

These results demonstrated that there is unexplored potential in the production of truly closed-cell PHs for the encapsulation (and the controlled release) of useful liquids and melts.

Phase change materials (PCMs) are substances that exhibit relatively large latent heats of phase transition (melting and crystallization) and can, therefore, be used to store and release large amounts of thermal energy. The thermal properties of PCMs can be harnessed for such applications as solar energy storage, electronic cooling, thermo-regulated textiles, energy efficient buildings, and food storage.[52] Such PCMs are classified into organic (paraffins and non-paraffins), inorganic (salt hydrates, metals, and inorganic compounds), and eutectic mixtures (organic–organic, organic–inorganic, and inorganic–inorganic). For effective application, several leak-proof PCM encapsulation techniques have been developed.[53,54] Depending on the size scale of the encapsulation technology, PCM encapsulations are classified into macro (>1 mm), micro (1–1000 μm), and nano (up to 1 μm).[53]

Micro- and nano-encapsulated PCMs exhibit higher heat transfer areas (higher surface-to-volume-ratios) and superior structural stabilities, and therefore, they are the most widely investigated systems for energy storage and release applications. Microencapsulated PCMs are produced using a variety of methods that are classified into physical (spray drying), physical–chemical (coacervation and sol–gel techniques), and chemical (interfacial, suspension, and emulsion polymerizations), processes that predominantly produce powders.[55–57] PCM microencapsulation has been effected using a variety of shell materials including acrylics,[58,59] melamine–formaldehyde resins,[60,61] urea-formaldehyde resins,[62,63] and poly (urethane urea)s (PUUs).[64–66] The PCM encapsulation capacity in these systems, and hence the amount of latent heat available, is limited by the low PCM contents in the micro- and nano-encapsulation systems.[67,68] The PUU interfacial step growth polymerization (ISGP) between isocyanates in the dispersed phase and water and/or polyols in the continuous phase is an elegant method of producing core–shell particles and has been applied in suspensions, miniemulsions, and microfluidic flows.[69–73] Monolithic encapsulation systems that provide higher PCM storage capacities, higher heat transfer areas, higher thermal conductivities, and structural robustness would be advantageous. Recently, an organic phase change material (~73 wt%) was encapsulated within a hydrogel PH based on the free radical polymerization of sodium acrylate within a Pickering HIPE.[44]

Here, the encapsulation of exceptionally large amounts of an organic PCM, ~90 wt%, within truly closed-cell PHs synthesized within oil-in-water (o/w) HIPEs using the advantageous ISGP is described for the first time. As shown in Fig. 1, crosslinked PUU PHs were synthesized through the ISGP of a renewable resource polyol (tannic acid, TA) and various isocyanates in the presence of water (producing both urethane and urea groups). Since the transition temperature of the encapsulated organic PCM (octadecane, OD) is near room temperature, the resulting PH is suitable for various "thermal comfort" applications.[74]

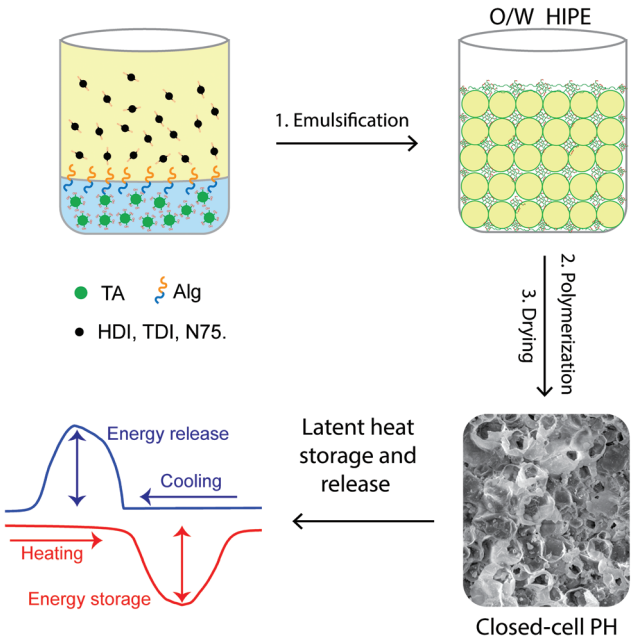

Fig. 1 A scheme illustrating the synthesis of PCM-encapsulating PHs for thermal energy storage and release applications through ISGP within a HIPE.

Experimental

Materials

The external aqueous phase contained TA (Aldrich, puriss), which served as the water-soluble polyol, and sodium alginate (Alg, Aldrich, from brown algae), which served as a reactive surfactant (the structures are illustrated in Fig. 2). The major part of the internal organic phase was comprised of OD (99.0%, Aldrich). The organic-soluble isocyanates (shown in Fig. 2) were hexamethylene diisocyanate (HDI, ≥98.0%, Aldrich), 2,4-toluene diisocyanate (TDI, 95.0%, Aldrich), and Desmodur© N75 (kindly donated by Tambour Ltd, Israel). While both TA and Alg will react with the isocyanates, the term "polyol" is used to describe TA since it is the dominant component. Dibutyltin dilaurate (DBTDL, 95.0%, Aldrich) was used as the polymerization catalyst. Unless stated otherwise, the materials were used as received. Deionized water was used throughout.

Polymer synthesis

The PHs are denoted TA/HDI, TA/TDI, and TA/N75, where TA represents the polyol and HDI, TDI, N75 represent the isocyanates. The synthesis of the PUU PHs took place in o/w HIPEs with the aqueous external phase consisting of deionized water (21.95 wt%), the reactive surfactant (Alg, 0.50 wt%), and the polyol (TA, 2.49 wt%). The organic internal phase was added to the external phase in three separate stages: first the PCM (OD, 72.32 wt%), then the isocyanate (2.49 wt%), and finally, the catalyst (DBTDL, 0.25 wt%). The volume ratio between the aqueous external phase and the organic internal phase was 1.00/4.08. The staged addition of

Published on 08 febrero 2019. Downloaded on 24/10/2025 02:32:36 a. m..

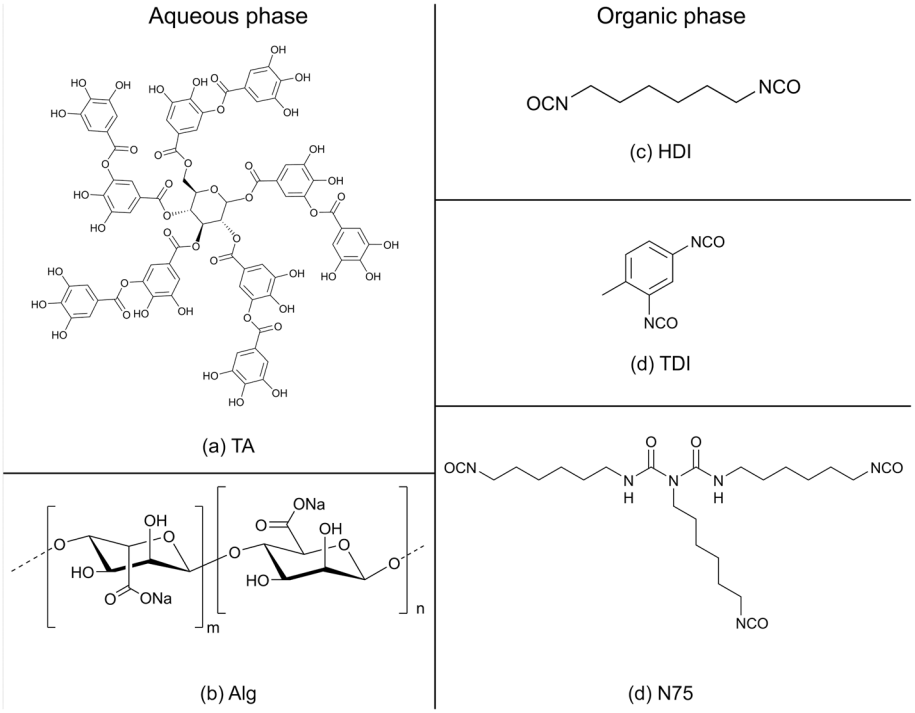

Fig. 2 Structures of the aqueous phase components: (a) TA; (b) Alg. Structures of the isocyanates in the organic phase: (c) HDI; (d) TDI; (e) N75.

the internal phase (PCM, isocyanate, catalyst) was used to prevent premature reaction of the isocyanate with the aqueous phase components. The aqueous phase (100 mL beaker) was placed in a water bath at 30 °C to regulate the temperature and was stirred with a mechanical stirrer (Heidolph RZR 2052) at 200 rpm. The HIPE was generated by adding the OD dropwise, at approximately 15 drops per minute, to the aqueous phase with constant stirring. The isocyanate was then added dropwise, after which the HIPE was stirred for an additional minute. The catalyst was then added dropwise with additional stirring. The resulting HIPE, a viscous, yellowish-white paste, was covered with aluminum foil and then polymerized in a circulating air oven at 37 °C for 24 h. The resulting PH was dried in a vacuum oven at room temperature for around 48 h (until a constant weight was achieved). A stable HIPE could not be produced without the Alg and a capsule-like structure could not be produced without the TA. Given the multiplicity of groups in both TA and Alg that are available to react with the isocyanate, it is clear that all the TA and all the Alg were incorporated into the polymeric structure.

Characterization

The structures of the PHs were characterized using scanning electron microscopy (SEM) (FEI E-SEM Quanta 200, secondary electron detector). Cryogenic fracture surfaces, obtained by immersing the PH samples in liquid nitrogen before fracture were coated with a gold–palladium layer (Polaron gold coater). The average OD droplet diameters were calculated by measuring 50 to 90 droplets in the SEM micrographs (the droplet diameter distributions are presented in Fig. S1, ESI†). The average droplet diameter was corrected for the random nature of the section by multiplying by $2/(3^{1/2})$.[75] The molecular structures were characterized using Fourier transform infrared spectroscopy (FTIR) in transmission (Bruker Equinox 55 FTIR spectrometer) with a resolution of 4 cm^{-1} in absorbance. Approximately 0.001 g of the sample was ground with approximately 0.3 g KBr and pressed into pellets for FTIR. A spectrum from the PUU that forms the encapsulating shells was obtained by removing the OD (dispersing a finely ground PH in *n*-hexane, stirring overnight at room temperature, decanting the supernatant, and washing a second time with *n*-hexane). Finally, the resulting PUU shell was vacuum dried for at least 3 h at room temperature.

The OD ignition (flash point) and the degradation of the encapsulating polymer were investigated using thermogravimetric analysis (TGA, TA TGA-Q50), with the samples heated from room temperature to 600 °C at 10 °C min^{-1} under air. The mass fraction of OD in the PH (m_{OD}) was determined from the TGA mass loss that was ascribed to the OD. The OD crystallization and melting were investigated using differential scanning calorimetry (DSC, TA DSC-Q20), heating from −10 °C to 100 °C at 10 °C min^{-1} in air (1st heating) and then cooling from 100 °C to −10 °C at 10 °C min^{-1} (1st cooling) to complete the first thermal cycle. Four cycles were used to demonstrate thermal reversibility and the results presented here were taken from the 1st cooling and the 2nd heating. The thermal analysis results included the OD melting temperature (T_m), the OD crystallization temperatures (T_c), the width of the melting range (ΔT_m), the width of the crystallization range (ΔT_c), and the heats from OD melting and crystallization (ΔH_m and

 This journal is © The Royal Society of Chemistry 2019

Published on 08 febrero 2019. Downloaded on 24/10/2025 02:32:36 a. m..

ΔH_c, respectively). ΔT_m was obtained from the onset and end of OD melting and ΔT_c was obtained from the onset and end of OD crystallization.

Compressive stress–strain measurements were performed on the PHs using an Instron 3345. The samples (approximately 7 mm × 7 mm × 7 mm) were cut from the PH monoliths. The measurements were performed at room temperature at a strain rate of 10% min^{-1} until a strain of 70% was reached (machine limitation). The static compressive modulus (E) was calculated from the linear slope of the stress–strain curve at low strains. The stress at 70% strain, σ_{70}, which reflected the resistance to densification at 70% strain, was also determined from the stress–strain curve.

Results and discussion

Morphology

The structures of TA/HDI, TA/TDI, and TA/N75 are presented in Fig. 3. TA/HDI and TA/TDI exhibit capsule-like, closed-cell-like structures with an average capsule size of ~20 and 32 μm, respectively. TA/N75, on the other hand, exhibits a different morphology, combining capsules with a layer-like, open-cell structure. As expected from the open-cell structure of TA/N75, the OD leaked when it was heated above the OD melting point. Surprisingly, the OD also leaked from the seemingly closed-cell structure of TA/TDI when it was heated above the OD melting point, indicating that the PH structure was not truly closed-cell. The OD did not leak from TA/HDI, even when heated above the OD melting point (50 °C) for 30 min, confirming that it has a truly closed-cell structure. TA/HDI was, therefore, judged as the only PH suitable for practical application. The effects of the macromolecular structure and the nature of the PH's structure on the PH's thermal and mechanical properties are quite informative regarding the synthesis of such systems.

Macromolecular structure

The FTIR spectrum of TA/HDI is presented along with the spectra for TA and OD in Fig. 4. HDI reacts with TA and Alg to produce urethane groups and reacts with water to produce urea groups. The TA/HDI bands associated with the PUU, however, are much lower in intensity than the bands associated with OD, which comprises ~90% of the PH (TGA results, below). Therefore, the encapsulated OD was removed from the PH to obtain an FTIR spectrum from TA/HDI's PUU shell. The bands corresponding to both the urethane and the urea groups, seen in other PUU PHs, are also observed in TA/HDI.[10] The >C═O stretching bands associated with urethane (UT) and urea (UA) were observed at 1731 and 1627 cm^{-1}, respectively. TA/HDI also exhibits bands associated with the urea CNH at 1576 cm^{-1}, with the urethane CN stretching at 1255 cm^{-1}, and with NH stretching (a broad band at around 3333 cm^{-1}). There is no evidence of the isocyanate band at 2260 cm^{-1}, indicating that there are no residual isocyanate groups in TA/HDI.

Thermal properties

OD content and degradation. The mass loss as function of temperature for OD and for the three PHs are presented in the TGA thermograms in Fig. 5, with the OD mass fractions in the PHs that were determined from the TGA results listed in

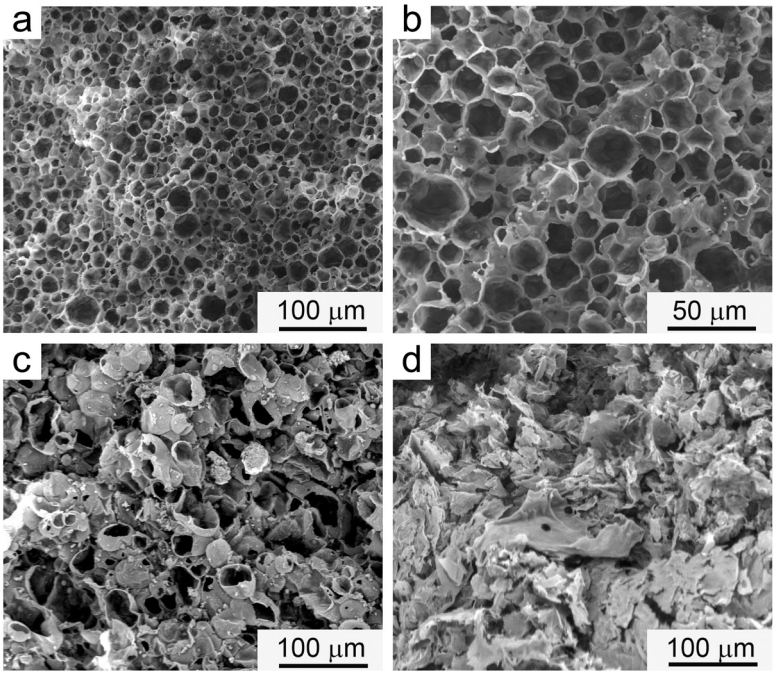

Fig. 3 Structures (SEM) of the PH monoliths: (a, b) TA/HDI; (c) TA/TDI; (d) TA/N75.

Published on 08 febrero 2019. Downloaded on 24/10/2025 02:32:36 a. m..

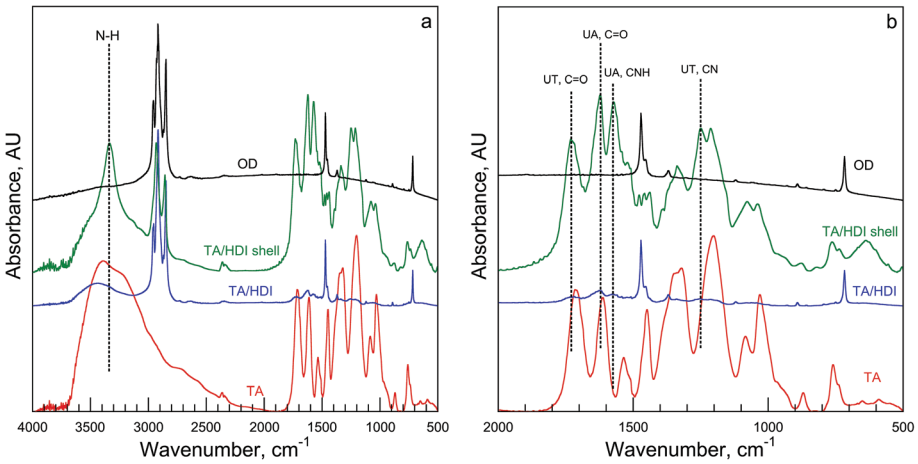

Fig. 4 FTIR spectra from OD, TA, and TA/HDI (both the OD-filled PH and the PUU shell): (a) spectra from 500 to 4000 cm^{-1}; (b) spectra from 500 to 2000 cm^{-1} showing the main urethane and urea bands.

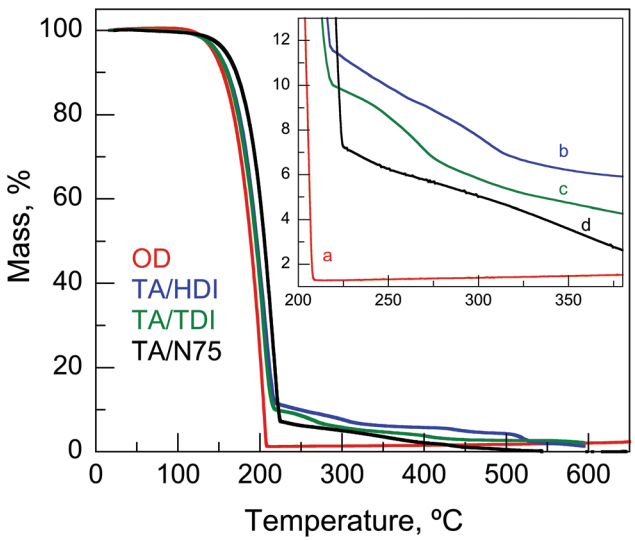

Fig. 5 Thermal decomposition in air (TGA) of: (a) OD; (b) TA/HDI; (c) TA/TDI; (d) TA/N75. Inset: enlargement of the results at low residual masses.

Table 1 PH compositions and a summary of the thermal and mechanical properties

	OD	TA/HDI	TA/TDI	TA/N75
m_{OD}, wt%	100	90	90	92
T_{c1}, °C	26	16	21	22
ΔT_{c1}, °C	6.2	20.0	15.0	14.0
ΔH_{c1}, J g_{sample}^{-1}	250	211	206	204
T_{m2}, °C	32	35	32	30
ΔT_{m2}, °C	10.1	31.0	22.0	21.0
ΔH_{m2}, J g_{sample}^{-1}	248	215	201	209
E, MPa	NA	6.7	1.0	0.19
σ_{70}, MPa	NA	20	3.4	0.54
ξ, %	NA	85.5	81.7	82.9
ξ_{eff}, %	NA	95.0	90.8	90.1

Table 1. The mass loss occurred in two obvious stages (Fig. 5), with the first mass loss stage ascribed to the ignition of the encapsulated OD. Pristine OD ignites at around 203 °C and the OD encapsulated within TA/HDI, TA/TDI, or TA/N75 ignited at somewhat higher temperatures. The mass losses upon OD ignition indicate that the OD contents in the PHs are around 90 wt% (Table 1), significantly higher than those achieved using micro- and nano-encapsulation (50 to 80%).[76–78] The second mass loss stage is ascribed to the degradation of the encapsulating polymer, which varied somewhat with the nature of the isocyanate (Fig. 5, inset). Degradation began for the HDI-, TDI-, and N75-based PHs at 305, 266, and 354 °C, respectively. The higher degradation temperature for TA/N75 reflects N75's isocyanate functionality of 3, which increases the extent of crosslinking.

OD crystallization and melting. DSC thermograms from OD and from the three PHs are presented in Fig. 6. The thermal behavior of TA/HDI is quite different from those of the other PHs. TA/HDI exhibits significantly broader crystallization and melting peaks, with lower peak values, than the other two PHs. Interestingly, the OD transition temperatures, the transition temperature ranges, and the energy that is stored or released are strongly dependent upon the nature of isocyanate and the resulting macromolecular and porous structures. TA/TDI and TA/N75 had T_cs (21 and 22 °C, respectively) which were slightly lower than that of the pristine OD (26 °C). The T_c of TA/HDI (16 °C), on the other hand, was significantly lower than that of the pristine OD. The truly closed-cell structure of TA/HDI exhibited a larger transition temperature range (ΔT_c, around 20 °C) than those of TA/TDI and TA/N75 (around 14 °C) and a significantly larger ΔT_c than that of pristine OD (~6 °C). TA/TDI and TA/N75 had T_ms (32 and 30 °C, respectively) were similar to that of pristine OD (32 °C). The T_m of TA/HDI (35 °C), on the other hand, was somewhat higher and the ΔT_m was somewhat broader. The encapsulation of OD within the micrometer-sized capsules of the PH has a signifi-

 This journal is © The Royal Society of Chemistry 2019

Published on 08 febrero 2019. Downloaded on 24/10/2025 02:32:36 a. m..

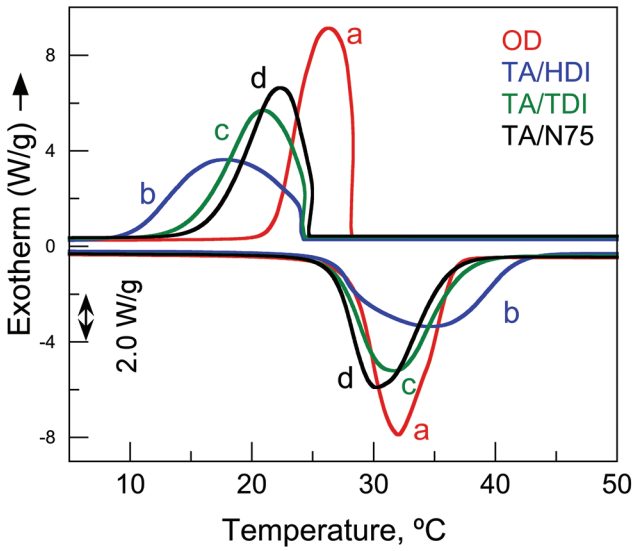

Fig. 6 Thermal behavior (DSC) from the first cooling and the second heating of: (a) OD; (b) TA/HDI; (c) TA/TDI; (d) TA/N75.

cant effect on the thermal behavior associated with OD, lowering the T_c, raising the T_m, and broadening the transitions. All three of the PHs exhibited similar energy storage capacities, latent heats of crystallization of ~207 J g_{sample}^{-1}.

The performance of the encapsulated OD for heat storage and release was described using two parameters, the encapsulation efficiency (ξ) and the effective encapsulation efficiency (ξ_{eff}) (eqn (1) and (2), respectively).[79,80] ξ compares the performance of the PH encapsulation system to the performance of pristine OD.[80,81] ξ_{eff} compares the performance of the OD within the PH encapsulation system to the performance of pristine OD. All three PHs exhibited ξ that were greater than 80% and ξ_{eff} that were greater than 90% (Table 1) with TA/HDI exhibiting the highest ξ (85.5%) and ξ_{eff} (95.0%). These high efficiencies demonstrate that the thermal capacity of the PH system is quite close to that of OD and that encapsulation within the PH does not delitoriously affect the heat storage performace of the OD itself.

$$\xi = \frac{(\Delta H_m + \Delta H_c)_{sample}}{(\Delta H_m + \Delta H_c)_{OD}} \quad (1)$$

$$\xi_{eff} = \frac{\xi}{m_{OD}} \quad (2)$$

Mechanical robustness

Mechanical robustness is essential for the long-term stability of a leak-proof encapsulation system. During handling, TA/HDI and TA/TDI seemed relatively robust, while TA/N75 was relatively brittle and crumbled easily. PHs that possess highly interconnected, open-cell porous structures typically have compressive stress–strain curves that exhibit three distinct regions: a linear elastic region at low strains (from which the Young's modulus is derived); a stress plateau region during an accordion-like collapse; and a densification or crushing region at high strains that is characterized by a rapid increase in stress. These OD-encapsulating PHs, however, are not porous, but instead, consist of closed-cell capsules. Therefore, the mechanical behavior of these PHs is expected to be different from that of typical, open-cell PHs.

The compressive stress–strain curves from the three PHs are presented in Fig. 7 and the mechanical properties derived therefrom are summarized in Table 1. Interestingly, TA/TDI and TA/N75 exhibit stress–strain curves that are similar to those of elastomeric open-cell foams.[8] The solid OD was easily squeezed out of TA/TDI and TA/N75 during the compression test, offering little resistance to the applied strain. Therefore, the PHs possessed significantly lower moduli (1.0 and 0.19 MPa, respectively) and significantly lower stresses at 70% strain (3.4 and 0.54 MPa, respectively) compared to TA/HDI. TA/N75 has a significantly lower modulus and a significantly lower σ_{70} than TA/TDI, reflecting its more open-cell structure (Fig. 3d) and its more brittle nature, producing multiple internal fractures during deformation rather than the fracture of the entire sample. There was no shape recovery once the stress was removed.

The encapsulated solid OD was not squeezed out of TA/HDI at low compressive strains. The successful OD encapsulation limited the PH deformation, resisting the applied strain and producing a relatively rapid increase in stress. This relatively high resistance to compression produces a relatively high modulus (6.7 MPa) and a relatively high σ_{70} (20 MPa) compared to the PHs from which the OD was easily squeezed out in response to the applied strain. The mechanical behavior of the truly closed-cell TA/HDI was similar to those seen for the elastomeric, water-encapsulating, truly closed-cell PHs synthesized within water-in-oil HIPEs. Here, however, there was no shape recovery once the stress was removed.[8] Interestingly, it is the influence of the truly closed-cell structure formed

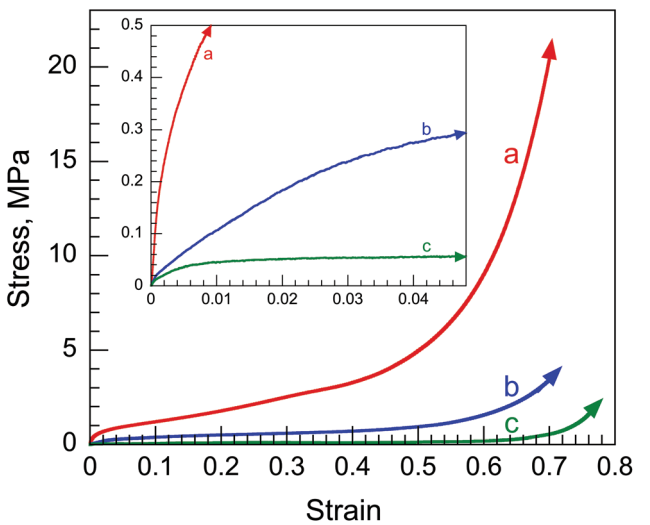

Fig. 7 Compressive stress–strain curves from: (a) TA/HDI; (b) TA/TDI; (c) TA/N75. Inset: enlargement of the results at low strains.

Published on 08 febrero 2019. Downloaded on 24/10/2025 02:32:36 a. m..

using aliphatic HDI that dominates the mechanical properties rather than the stiffer macromolecular structure that is formed when using aromatic TDI and rather than the stiffer, highly crosslinked macromolecular structure that is formed when using the tri-functional N75. It is the more flexible macromolecular structure produced with HDI that enables the successful encapsulation of the OD and the associated efficient thermal energy storage and robust mechanical behavior.

Conclusions

Exceptionally large amounts (~90 wt%, as determined using TGA) of OD, an organic PCM, were encapsulated as micrometer-scale droplets within truly closed-cell PHs synthesized within oil-in-water HIPEs through interfacial step growth polymerization. The poly(urethane urea) PHs were synthesized using tannic acid (polyol) and sodium alginate (reactive surfactant) in the aqueous external phase and using an isocyanate in the organic internal phase (which was largely OD). TA/HDI, the PH based on hexamethylene diisocyanate, exhibited a truly closed-cell structure with a relatively high thermal energy storage capacity (211 J g_{sample}^{-1}), a relatively high encapsulation efficiency (85.5%), and a relatively high effective encapsulation efficiency (95.0%). The truly closed-cell structure produced thermal behavior in the PH that was different from that of pristine OD (a lower crystallization point, a higher melting point, and broader transitions). TA/HDI was mechanically robust, with a relatively high compressive modulus (6.7 MPa) and a relatively high stress at 70% strain (20 MPa) compared to the PHs based on other isocyanates from which the OD was squeezed out on application of strain. Interestingly, it is the more flexible macromolecular structure produced with HDI that enables the successful encapsulation of the OD and the associated efficient thermal energy storage and robust mechanical behavior. The encapsulation of such exceptionally high PCM contents within individual micrometer-scale capsules in mechanically robust monoliths will be essential for any practical application.

Conflicts of interest

There are no conflicts of interest to declare.

Acknowledgements

The authors gratefully acknowledge the partial support of the Israel Science Foundation (294/12 and 519/16) and the Israel Ministry of Science (880011).

Notes and references

1 N. R. Cameron and D. C. Sherrington, High Internal Phase Emulsions (HIPEs)-Structure, Properties and Use in Polymer Preparation, *Adv. Polym. Sci.*, 1996, **126**, 163.
2 M. S. Silverstein, Emulsion-templated polymers: Contemporary contemplations, *Polymer*, 2017, **126**, 261.
3 M. S. Silverstein, PolyHIPEs: Recent advances in emulsion-templated porous polymers, *Prog. Polym. Sci.*, 2014, **39**, 199.
4 M. S. Silverstein, Emulsion-templated porous polymers: A retrospective perspective, *Polymer*, 2014, **55**, 304.
5 A. Khodabandeh, R. D. Arrua, F. R. Mansour, S. C. Thickett and E. F. Hilder, PEO-based brush-type amphiphilic macro-RAFT agents and their assembled polyHIPE monolithic structures for applications in separation science, *Sci. Rep.*, 2017, **7**, 7847.
6 A. Khodabandeh, R. D. Arrua, C. T. Desire, T. Rodemann, S. A. F. Bon, S. C. Thickett and E. F. Hilder, Preparation of inverse polymerized high internal phase emulsions using an amphiphilic macro-RAFT agent as sole stabilizer, *Polym. Chem.*, 2016, **7**, 1803.
7 I. Gurevitch and M. S. Silverstein, Nanoparticle-Based and Organic-Phase-Based AGET ATRP PolyHIPE Synthesis within Pickering HIPEs and Surfactant-Stabilized HIPEs, *Macromolecules*, 2011, **44**, 3398.
8 I. Gurevitch and M. S. Silverstein, One-Pot Synthesis of Elastomeric Monoliths Filled with Individually Encapsulated Liquid Droplets, *Macromolecules*, 2012, **45**, 6450.
9 I. Barbara, M.-A. Dourges and H. Deleuze, Preparation of porous polyurethanes by emulsion-templated step growth polymerization, *Polymer*, 2017, **132**, 243.
10 D. David and M. S. Silverstein, Porous polyurethanes synthesized within high internal phase emulsions, *J. Polym. Sci., Part A: Polym. Chem.*, 2009, **47**, 5806.
11 S. Livshin and M. S. Silverstein, Cross-linker flexibility in porous crystalline polymers synthesized from long side-chain monomers through emulsion templating, *Soft Matter*, 2008, **4**, 1630.
12 N. Cohen and M. S. Silverstein, One-Pot Emulsion-Templated Synthesis of an Elastomer-Filled Hydrogel Framework, *Macromolecules*, 2012, **45**, 1612.
13 J. Normatov and M. S. Silverstein, Highly porous elastomer-silsesquioxane nanocomposites synthesized within high internal phase emulsions, *J. Polym. Sci., Part A: Polym. Chem.*, 2008, **46**, 2357.
14 J. Normatov and M. S. Silverstein, Interconnected Silsesquioxane–Organic Networks in Porous Nanocomposites Synthesized within High Internal Phase Emulsions, *Chem. Mater.*, 2008, **20**, 1571.
15 S. Ungureanu, M. Birot, G. Laurent, H. Deleuze, O. Babot, B. Julian-Lopez, M. F. Achard, M. I. Popa, C. Sanchez and R. Backov, One-Pot Syntheses of the First Series of Emulsion Based Hierarchical Hybrid Organic–Inorganic Open-Cell Monoliths Possessing Tunable Functionality (Organo–Si(HIPE) Series), *Chem. Mater.*, 2007, **19**, 5786.
16 M. Turnšek, P. Krajnc, R. Liska and T. Koch, Macroporous alumina with cellular interconnected morphology from emulsion templated polymer composite precursors, *J. Eur. Ceram. Soc.*, 2016, **36**, 1045.

 This journal is © The Royal Society of Chemistry 2019

Published on 08 febrero 2019. Downloaded on 24/10/2025 02:32:36 a. m..

17 S. Kovačič and M. S. Silverstein, Hydrogels through emulsion templating: sequential polymerization and double networks, *Polym. Chem.*, 2017, **8**, 6319.
18 F. Carn, A. Colin, M.-F. Achard, H. Deleuze, E. Sellier, M. Birot and R. Backov, Inorganic monoliths hierarchically textured via concentrated direct emulsion and micellar templates, *J. Mater. Chem.*, 2004, **14**, 1370.
19 N. Brun, S. R. S. Prabaharan, M. Morcrette, C. Sanchez, G. Pécastaings, A. Derré, A. Soum, H. Deleuze, M. Birot and R. Backov, Hard Macrocellular Silica Si(HIPE) Foams Templating Micro/Macroporous Carbonaceous Monoliths: Applications as Lithium Ion Battery Negative Electrodes and Electrochemical Capacitors, *Adv. Funct. Mater.*, 2009, **19**, 3136.
20 L. L. C. Wong, S. Barg, A. Menner, P. do Vale Pereira, G. Eda, M. Chowalla, E. Saiz and A. Bismarck, Macroporous polymer nanocomposites synthesised from high internal phase emulsion templates stabilised by reduced graphene oxide, *Polymer*, 2014, **55**, 395.
21 A. Menner, M. Salgueiro, M. S. P. Shaffer and A. Bismarck, Nanocomposite foams obtained by polymerization of high internal phase emulsions, *J. Polym. Sci., Part A: Polym. Chem.*, 2008, **46**, 5708.
22 A. Menner, R. Verdejo, M. Shaffer and A. Bismarck, Particle-Stabilized Surfactant-Free Medium Internal Phase Emulsions as Templates for Porous Nanocomposite Materials: poly-Pickering-Foams, *Langmuir*, 2007, **23**, 2398.
23 N. Cohen, D. C. Samoocha, D. David and M. S. Silverstein, Carbon nanotubes in emulsion-templated porous polymers: Polymer nanoparticles, sulfonation, and conductivity, *J. Polym. Sci., Part A: Polym. Chem.*, 2013, **51**, 4369.
24 R. T. Woodward, F. Markoulidis, F. De Luca, D. B. Anthony, D. Malko, T. O. McDonald, M. S. P. Shaffer and A. Bismarck, Carbon foams from emulsion-templated reduced graphene oxide polymer composites: electrodes for supercapacitor devices, *J. Mater. Chem. A*, 2018, **6**, 1840.
25 N. Brun, S. R. S. Prabaharan, C. Surcin, M. Morcrette, H. Deleuze, M. Birot, O. Babot, M. F. Achard and R. Backov, Design of Hierarchical Porous Carbonaceous Foams from a Dual-Template Approach and Their Use as Electrochemical Capacitor and Li Ion Battery Negative Electrodes, *J. Phys. Chem. C*, 2012, **116**, 1408.
26 K. Kapilov-Buchman, L. Portal, Y. Zhang, N. Fechler, M. Antonietti and M. S. Silverstein, Hierarchically porous carbons from an emulsion-templated, urea-based deep eutectic, *J. Mater. Chem. A*, 2017, **5**, 16376.
27 S. Israel, I. Gurevitch and M. S. Silverstein, Carbons with a hierarchical porous structure through the pyrolysis of hypercrosslinked emulsion-templated polymers, *Polymer*, 2015, **72**, 453.
28 R. T. Woodward, A. Jobbe-Duval, S. Marchesini, D. B. Anthony, C. Petit and A. Bismarck, Hypercrosslinked polyHIPEs as precursors to designable, hierarchically porous carbon foams, *Polymer*, 2017, **115**, 146.
29 R. S. Moglia, J. L. Holm, N. A. Sears, C. J. Wilson, D. M. Harrison and E. Cosgriff-Hernandez, Injectable PolyHIPEs as High-Porosity Bone Grafts, *Biomacromolecules*, 2011, **12**, 3621.
30 W. Busby, N. R. Cameron and C. A. B. Jahoda, Emulsion-Derived Foams (PolyHIPEs) Containing Poly(ε-caprolactone) as Matrixes for Tissue Engineering, *Biomacromolecules*, 2001, **2**, 154.
31 R. S. Moglia, M. Whitely, P. Dhavalikar, J. Robinson, H. Pearce, M. Brooks, M. Stuebben, N. Cordner and E. Cosgriff-Hernandez, Injectable Polymerized High Internal Phase Emulsions with Rapid in Situ Curing, *Biomacromolecules*, 2014, **15**, 2870.
32 Y. Lumelsky, I. Lalush-Michael, S. Levenberg and M. S. Silverstein, A degradable, porous, emulsion-templated polyacrylate, *J. Polym. Sci., Part A: Polym. Chem.*, 2009, **47**, 7043.
33 M. Paljevac, L. Gradišnik, S. Lipovšek, U. Maver, J. Kotek and P. Krajnc, Multiple-Level Porous Polymer Monoliths with Interconnected Cellular Topology Prepared by Combining Hard Sphere and Emulsion Templating for Use in Bone Tissue Engineering, *Macromol. Biosci.*, 2018, **18**, 1700306.
34 F. Fernández-Trillo, J. C. M. v. Hest, J. C. Thies, T. Michon, R. Weberskirch and N. R. Cameron, Reversible Immobilization onto PEG-based Emulsion-templated Porous Polymers by Co-assembly of Stimuli Responsive Polymers, *Adv. Mater.*, 2009, **21**, 55.
35 W. Li, W. Zhang, X. Dong, L. Yan, R. Qi, W. Wang, Z. Xie and X. Jing, Porous heterogeneous organic photocatalyst prepared by HIPE polymerization for oxidation of sulfides under visible light, *J. Mater. Chem.*, 2012, **22**, 17445.
36 E. Yüce, E. H. Mert, P. Krajnc, F. N. Parın, N. San, D. Kaya and H. Yıldırım, Photocatalytic Activity of Titania/Polydicyclopentadiene PolyHIPE Composites, *Macromol. Mater. Eng.*, 2017, **302**, 1700091.
37 I. Pulko, M. Kolar and P. Krajnc, Atrazine removal by covalent bonding to piperazine functionalized PolyHIPEs, *Sci. Total Environ.*, 2007, **386**, 114.
38 S. Huš, M. Kolar and P. Krajnc, Separation of heavy metals from water by functionalized glycidyl methacrylate poly (high internal phase emulsions), *J. Chromatogr. A*, 2016, **1437**, 168.
39 T. Zhang and M. S. Silverstein, Doubly-crosslinked, emulsion-templated hydrogels through reversible metal coordination, *Polymer*, 2017, **126**, 386.
40 I. Gurevitch and M. S. Silverstein, Shape memory polymer foams from emulsion templating, *Soft Matter*, 2012, **8**, 10378.
41 C. Warwar Damouny and M. S. Silverstein, Hydrogel-filled, semi-crystalline, nanoparticle-crosslinked, porous polymers from emulsion templating: Structure, properties, and shape memory, *Polymer*, 2016, **82**, 262.
42 F. Du, L. Sun, X. Zhen, H. Nie, Y. Zheng, G. Ruan and J. Li, High-internal-phase-emulsion polymeric monolith coupled with liquid chromatography–electrospray tandem mass spectrometry for enrichment and sensitive detection of

Published on 08 febrero 2019. Downloaded on 24/10/2025 02:32:36 a. m..

trace cytokinins in plant samples, *Anal. Bioanal. Chem.*, 2015, **407**, 6071.
43 A. Khodabandeh, R. D. Arrua, F. R. Mansour, S. C. Thickett and E. F. Hilder, PEO-based brush-type amphiphilic macro-RAFT agents and their assembled polyHIPE monolithic structures for applications in separation science, *Sci. Rep.*, 2017, **7**, 7847.
44 H. Gui, T. Zhang and Q. Guo, Closed-cell, emulsion-templated hydrogels for latent heat storage applications, *Polym. Chem.*, 2018, **9**, 3970.
45 J. A. M. Balderrama, M.-A. Dourges, A. Magueresse, L. Maheo, H. Deleuze and P. Glouannec, Emulsion-templated pullulan monoliths as phase change materials encapsulating matrices, *Mater. Today Commun.*, 2018, **17**, 466–473.
46 A. Quell, B. de Bergolis, W. Drenckhan and C. Stubenrauch, How the Locus of Initiation Influences the Morphology and the Pore Connectivity of a Monodisperse Polymer Foam, *Macromolecules*, 2016, **49**, 5059.
47 J. M. Williams and D. A. Wrobleski, Spatial distribution of the phases in water-in-oil emulsions. Open and closed microcellular foams from cross-linked polystyrene, *Langmuir*, 1988, **4**, 656.
48 P. Viswanathan, D. W. Johnson, C. Hurley, N. R. Cameron and G. Battaglia, 3D Surface Functionalization of Emulsion-Templated Polymeric Foams, *Macromolecules*, 2014, **47**, 7091.
49 A. Khodabandeh, R. Dario Arrua, C. T. Desire, T. Rodemann, S. A. F. Bon, S. C. Thickett and E. F. Hilder, Preparation of inverse polymerized high internal phase emulsions using an amphiphilic macro-RAFT agent as sole stabilizer, *Polym. Chem.*, 2016, **7**, 1803.
50 I. Gurevitch and M. S. Silverstein, Polymerized Pickering HIPEs: Effects of synthesis parameters on porous structure, *J. Polym. Sci., Part A: Polym. Chem.*, 2010, **48**, 1516.
51 E. M. Christenson, W. Soofi, J. L. Holm, N. R. Cameron and A. G. Mikos, Biodegradable Fumarate-Based PolyHIPEs as Tissue Engineering Scaffolds, *Biomacromolecules*, 2007, **8**, 3806.
52 C. Y. Zhao and G. H. Zhang, Review on microencapsulated phase change materials (MEPCMs): Fabrication, characterization and applications, *Renewable Sustainable Energy Rev.*, 2011, **15**, 3813.
53 P. B. Salunkhe and P. S. Shembekar, A review on effect of phase change material encapsulation on the thermal performance of a system, *Renewable Sustainable Energy Rev.*, 2012, **16**, 5603.
54 W. Su, J. Darkwa and G. Kokogiannakis, Review of solid–liquid phase change materials and their encapsulation technologies, *Renewable Sustainable Energy Rev.*, 2015, **48**, 373.
55 J. Giro-Paloma, M. Martínez, L. F. Cabeza and A. I. Fernández, Types, methods, techniques, and applications for microencapsulated phase change materials (MPCM): A review, *Renewable Sustainable Energy Rev.*, 2016, **53**, 1059.
56 G. Alva, Y. Lin, L. Liu and G. Fang, Synthesis, characterization and applications of microencapsulated phase change materials in thermal energy storage: A review, *Energy Build.*, 2017, **144**, 276.
57 X. Huang, C. Zhu, Y. Lin and G. Fang, Thermal properties and applications of microencapsulated PCM for thermal energy storage: A review, *Appl. Therm. Eng.*, 2019, **147**, 841.
58 C. Alkan and A. Sari, Fatty acid/poly(methyl methacrylate) (PMMA) blends as form-stable phase change materials for latent heat thermal energy storage, *Sol. Energy*, 2008, **82**, 118.
59 C. Alkan, A. Sarı, A. Karaipekli and O. Uzun, Preparation, characterization, and thermal properties of microencapsulated phase change material for thermal energy storage, *Sol. Energy Mater. Sol. Cells*, 2009, **93**, 143.
60 H. Zhang and X. Wang, Fabrication and performances of microencapsulated phase change materials based on n-octadecane core and resorcinol-modified melamine–formaldehyde shell, *Colloids Surf., A*, 2009, **332**, 129.
61 J. Su, L. Wang and L. Ren, Fabrication and thermal properties of microPCMs: Used melamine-formaldehyde resin as shell material, *J. Appl. Polym. Sci.*, 2006, **101**, 1522.
62 N. Sarier and E. Onder, The manufacture of microencapsulated phase change materials suitable for the design of thermally enhanced fabrics, *Thermochim. Acta*, 2007, **452**, 149.
63 J.-P. Wang, X.-P. Zhao, H.-L. Guo and Q. Zheng, Preparation of Microcapsules Containing Two-Phase Core Materials, *Langmuir*, 2004, **20**, 10845.
64 D. Saihi, I. Vroman, S. Giraud and S. Bourbigot, Microencapsulation of ammonium phosphate with a polyurethane shell. Part II. Interfacial polymerization technique, *React. Funct. Polym.*, 2006, **66**, 1118.
65 C. Liang, X. Lingling, S. Hongbo and Z. Zhibin, Microencapsulation of butyl stearate as a phase change material by interfacial polycondensation in a polyurea system, *Energy Convers. Manage.*, 2009, **50**, 723.
66 Y. Yoo, C. Martinez and J. P. Youngblood, Synthesis and Characterization of Microencapsulated Phase Change Materials with Poly(urea–urethane) Shells Containing Cellulose Nanocrystals, *ACS Appl. Mater. Interfaces*, 2017, **9**, 31763.
67 Q. Wu, D. Zhao, X. Jiao, Y. Zhang, K. J. Shea, X. Lu and G. Qiu, Preparation, Properties, and Supercooling Prevention of Phase Change Material n-Octadecane Microcapsules with Peppermint Fragrance Scent, *Ind. Eng. Chem. Res.*, 2015, **54**, 8130.
68 Y. Zhu, S. Liang, K. Chen, X. Gao, P. Chang, C. Tian, J. Wang and Y. Huang, Preparation and properties of nanoencapsulated n-octadecane phase change material with organosilica shell for thermal energy storage, *Energy Convers. Manage.*, 2015, **105**, 908.
69 I. W. Cheong and J. H. Kim, Synthesis of core–shell polyurethane–urea nanoparticles containing 4,4′-methylenedi-p-phenyl diisocyanate and isophorone diisocyanate by self-assembled neutralization emulsification, *Chem. Commun.*, 2004, **21**, 2484.

 This journal is © The Royal Society of Chemistry 2019

Published on 08 febrero 2019. Downloaded on 24/10/2025 02:32:36 a. m..

70 F. Gaudin and N. Sintes-Zydowicz, Poly(urethane–urea) nanocapsules prepared by interfacial step polymerisation in miniemulsion: The droplet size: A key-factor for the molecular and thermal characteristics of the polymeric membrane of the nanocapsules?, *Colloids Surf., A*, 2011, **384**, 698.

71 V. Chiaradia, A. Valério, P. E. Feuser, D. D. Oliveira, P. H. H. Araújo and C. Sayer, Incorporation of superparamagnetic nanoparticles into poly(urea-urethane) nanoparticles by step growth interfacial polymerization in miniemulsion, *Colloids Surf., A*, 2015, **482**, 596.

72 W. Li, H. H. Pham, Z. Nie, B. MacDonald, A. Güenther and E. Kumacheva, Multi-Step Microfluidic Polymerization Reactions Conducted in Droplets: The Internal Trigger Approach, *J. Am. Chem. Soc.*, 2008, **130**, 9935.

73 I. Polenz, D. A. Weitz and J.-C. Baret, Polyurea Microcapsules in Microfluidics: Surfactant Control of Soft Membranes, *Langmuir*, 2015, **31**, 1127.

74 L. F. Cabeza, A. Castell, C. Barreneche, A. de Gracia and A. I. Fernández, Materials used as PCM in thermal energy storage in buildings: A review, *Renewable Sustainable Energy Rev.*, 2011, **15**, 1675.

75 A. Barbetta and N. R. Cameron, Morphology and Surface Area of Emulsion-Derived (PolyHIPE) Solid Foams Prepared with Oil-Phase Soluble Porogenic Solvents: Span 80 as Surfactant, *Macromolecules*, 2004, **37**, 3188–3201.

76 S. Liang, Q. Li, Y. Zhu, K. Chen, C. Tian, J. Wang and R. Bai, Nanoencapsulation of n-octadecane phase change material with silica shell through interfacial hydrolysis and polycondensation in miniemulsion, *Energy*, 2015, **93**, 1684.

77 Y. Zhu, S. Liang, H. Wang, K. Zhang, X. Jia, C. Tian, Y. Zhou and J. Wang, Morphological control and thermal properties of nanoencapsulated n-octadecane phase change material with organosilica shell materials, *Energy Convers. Manage.*, 2016, **119**, 151.

78 S. Liang, Y. Zhu, H. Wang, T. Wu, C. Tian, J. Wang and R. Bai, Preparation and Characterization of Thermoregulated Rigid Polyurethane Foams Containing Nanoencapsulated Phase Change Materials, *Ind. Eng. Chem. Res.*, 2016, **55**, 2721.

79 A. Sarı, C. Alkan, A. Karaipekli and O. Uzun, Microencapsulated n-octacosane as phase change material for thermal energy storage, *Sol. Energy*, 2009, **83**, 1757.

80 H. Zhang, X. Wang and D. Wu, Silica encapsulation of n-octadecane via sol–gel process: A novel microencapsulated phase-change material with enhanced thermal conductivity and performance, *J. Colloid Interface Sci.*, 2010, **343**, 246.

81 H. Zhang and X. Wang, Synthesis and properties of microencapsulated n-octadecane with polyurea shells containing different soft segments for heat energy storage and thermal regulation, *Sol. Energy Mater. Sol. Cells*, 2009, **93**, 1366.